



This is a repository copy of *The nature of the frequency spectrum of shear Alfvén waves in a solar coronal arcade*.

White Rose Research Online URL for this paper:
<http://eprints.whiterose.ac.uk/162722/>

Version: Accepted Version

Article:

Jain, R. orcid.org/0000-0002-0080-5445 (2020) The nature of the frequency spectrum of shear Alfvén waves in a solar coronal arcade. *Physics of Plasmas*, 27 (7). 072902. ISSN 1070-664X

<https://doi.org/10.1063/5.0002512>

This article may be downloaded for personal use only. Any other use requires prior permission of the author and AIP Publishing. This article appeared in (*Physics of Plasmas* 27, 072902 (2020); <https://doi.org/10.1063/5.0002512>) and may be found at (<https://aip.scitation.org/doi/full/10.1063/5.0002512>)

Reuse

Items deposited in White Rose Research Online are protected by copyright, with all rights reserved unless indicated otherwise. They may be downloaded and/or printed for private study, or other acts as permitted by national copyright laws. The publisher or other rights holders may allow further reproduction and re-use of the full text version. This is indicated by the licence information on the White Rose Research Online record for the item.

Takedown

If you consider content in White Rose Research Online to be in breach of UK law, please notify us by emailing eprints@whiterose.ac.uk including the URL of the record and the reason for the withdrawal request.



eprints@whiterose.ac.uk
<https://eprints.whiterose.ac.uk/>

This is the author's peer reviewed, accepted manuscript. However, the online version of record will be different from this version once it has been copyedited and typeset.

PLEASE CITE THIS ARTICLE AS DOI: 10.1063/5.0002512

The Nature of the Frequency Spectrum of Shear Alfvén waves in a Solar Coronal Arcade

Rekha Jain^{1, a)}

*School of Mathematics and Statistics, University of Sheffield (UK),
S3 7RH*

(Dated: 13 June 2020)

Frequency power spectra are computed theoretically for shear Alfvén waves excited in a solar coronal arcade by two separate perturbations, a Cosine-modulated Gaussian perturbation and an impulsive driver. The arcade is assumed to consist of potential magnetic field lines embedded in a stratified plasma. It is shown that although the power spectra have discrete frequencies for each field line, a cumulative effect of many field lines of different widths/lengths in an arcade will be that of a continuous spectrum, if seen together as one entity. The nature of the frequency power spectra can constrain the size and the type of the driver.

^{a)}R.Jain@sheffield.ac.uk

I. INTRODUCTION

Solar coronal loop-tops are often clearly visible in the Extreme Ultra Violet (EUV) images of the solar corona with their footpoints believed to be anchored in the photosphere. Such loop-tops may oscillate in response to nearby flaring activity (e.g. Aschwanden et al. 1999) and the resulting period of oscillations may provide a useful diagnostic tool for understanding the physical characteristic of the loops when compared with theoretical models (e.g. Edwin and Roberts, 1983). A collection of many visible loops in the solar corona is referred to as a coronal arcade.

A common interpretation is that the coronal loop oscillations are Magneto-hydrodynamics (MHD) waves (Aschwanden et al. 1999; Nakariakov et al. 1999) and the normal modes of oscillation are studied in different magnetic field and density profiles, a combination of which represents a typical coronal magnetic configuration. In the past, the solar coronal loops have been generally modelled either as magnetic slabs (see for example, Roberts, 1981; Edwin and Roberts, 1982; De Groof and Goossens 2002; Terradas et al. 2007) or as magnetic flux tubes (Edwin and Roberts, 1983; Diaz et al. 2004).

Transverse loop oscillations have been observed in detail, with the Atmospheric Imaging Assembly (AIA) instrument (Lemen et al. 2012) on board the Solar Dynamics Observatory (SDO) (Pesnell et al. 2012) and the measured periods have been used to determine the Alfvén speeds in the loops (see for example, White and Verwichte, 2012). Transverse oscillations can be modelled as incompressible modes (Edwin and Roberts, 1983; Verwichte et al., 2004, Goossens et al. 2009) due to weak compression in the long-wavelength limit. They have also been modelled as interference of waves in a three-dimensional wave cavity (Hindman and Jain, 2015). Observationally, one can measure the period or frequency of a bundle of oscillating coronal loops and their decay time using the EUV images. Therefore, it is important to understand the excitation and damping mechanisms of transverse oscillations in solar coronal arcades on the basis of two measurements i.e. the observed power spectrum and the damping times, both of which are frequency dependent. There are many mechanisms suggested for damping of these oscillations. For example, resonant absorption (see Goossens et al. 2002; Hindman and Jain, 2018), phase mixing (Heyvarts and Priest, 1983) and K-H instability (see for example, Soler et al. 2008) are some of the popular mechanisms. The excitation mechanisms also need to be investigated in detail. Observationally, this requires

This is the author's peer reviewed, accepted manuscript. However, the online version of record will be different from this version once it has been copyedited and typeset.

PLEASE CITE THIS ARTICLE AS DOI: 10.1063/1.50002512

simultaneous multi-wavelength observations to track the propagation of waves through the different layers of the solar atmosphere. Theoretically, one needs to model coronal loops and study the excitation of oscillations using different excitation sources and their corresponding frequency power spectra. The comparison of observational and theoretical power spectra can then give us some insight into the size of the driver and the responsible mechanism of excitation.

The simplest magnetic field model for generating oscillations, within the MHD framework, is a potential magnetic field model. One such investigation was carried out by Oliver et al. (1993) who studied Alfvén and Fast MHD waves in a two-dimensional potential magnetic field with equilibrium gas pressure and density decreasing with height. Tarr (2017) then extended this study of Oliver et al. (1993) to estimate the frequency spectrum of Alfvén waves in a coronal arcade generated by a local Gaussian perturbation representing a small reconnection event. Oliver et al. (1993) had shown that the frequencies of the modes are shifted depending on the separation of loop footpoints and the parameter, δ , the ratio of the magnetic field to pressure scale height. Tarr (2017) calculated the frequency spectrum analytically and hence they only investigated the case of zero δ , i.e. for uniform pressure and density. For coronal conditions the value of δ is expected to be around 1 (see Oliver et al. 1993). Considering non-zero finite values of δ makes the coefficient non-constant in the governing equation and it becomes necessary to solve the equation numerically. This paper revisits the model of Tarr (2017) to compute frequency spectrum numerically for different values of the parameter δ . Two different drivers are chosen both of which vanish at the line-tied boundaries. One driver represents a small reconnective event at the top of the loop and the other one an impulsive driver such as a big flare (see e.g. Aschwanden et al., 1999; Jain et al. 2015; Li et al. 2017).

In Section 2, the models of Oliver et al. (1993) and Tarr (2017) are described and the governing equations for the transverse Alfvén waves derived. The eigenvalues and eigenfunctions are also computed subject to boundary conditions. Section 3 determines the power spectra arising from a Cosine modulated Gaussian perturbation at the loop-top. For comparison, we also show the power spectra for an impulsive driver. A brief summary and conclusions are then mentioned in Section 4.

II. THE MODEL

The model set-up considered for a coronal arcade in Cartesian coordinate system is as in Oliver et al. (1993).

A potential magnetic field, \mathbf{B}_0 , is assumed in an equilibrium atmosphere at rest where the plasma pressure, p_0 and the force due to gravity balance each other, i.e.

$$-\nabla p_0 + \mathbf{J}_0 \times \mathbf{B}_0 + \rho_0 \mathbf{g} = \mathbf{0}. \quad (1)$$

Here \mathbf{J}_0 is the current density.

Using

$$p_0(z) = p_0 e^{-\frac{z}{H_p}}, \quad (2)$$

for equilibrium plasma pressure with $H_p (= \frac{K_B T}{mg})$ as the pressure scale height in the vertical direction $\hat{\mathbf{z}}$, and

$$\rho_0(z) = \rho_0 e^{-\frac{z}{H_p}}, \quad (3)$$

for equilibrium density, we can show that

$$\mathbf{B}_0 = B_0 \left[\cos\left(\frac{x}{H_B}\right), 0, \sin\left(\frac{x}{H_B}\right) \right] e^{-z/H_B} \quad (4)$$

with $H_B (= \frac{2l}{\pi})$; with $2l$ as the separation between the footpoints) as the magnetic scale height.

A. The Linearised Momentum Equation

Assuming small perturbations to the equilibrium magnetic field and ignoring the perturbed pressure and gravitational forces, the linearised momentum equation for a force-free and inviscid plasma can be given by

$$\rho_0(z) \frac{\partial \mathbf{v}_1}{\partial t} = \frac{1}{\mu_0} [(\nabla \times \mathbf{B}_1) \times \mathbf{B}_0], \quad (5)$$

where μ_0 is the permeability in the vacuum. Here, \mathbf{v}_1 and \mathbf{B}_1 are the perturbed velocity and perturbed magnetic field respectively.

Differentiating the above equation with respect to time and using the linearised ideal induction equation, we obtain

$$\rho_0(z) \frac{\partial^2 \mathbf{v}_1}{\partial t^2} = \frac{1}{\mu_0} [\nabla \times \{\nabla \times (\mathbf{v}_1 \times \mathbf{B}_0)\}] \times \mathbf{B}_0. \quad (6)$$

Using the vector identities and considering invariance in $\hat{\mathbf{y}}$ direction, we can write the above equation as

$$\rho_0(z) \frac{\partial^2 \mathbf{v}_1}{\partial t^2} = \left(\nabla^2 (\mathbf{v}_1 \cdot \nabla A) \right) \nabla A + \left[(\mathbf{B}_0 \cdot \nabla)^2 v_y \right] \hat{\mathbf{y}}. \quad (7)$$

with v_y as the y -component of the perturbed velocity. Here, we have also used the fact that

$$\mathbf{B}_0 = \nabla A(x, z) \times \hat{\mathbf{y}} = \left(-\frac{\partial A}{\partial z}, 0, \frac{\partial A}{\partial x} \right).$$

Fourier analysing the perturbed quantity in time i.e. $v_1 \propto e^{i\omega t}$, we obtain

$$-\omega^2 \rho_0(z) \mathbf{v}_1 = \left(\nabla^2 (\mathbf{v}_1 \cdot \nabla A) \right) \nabla A + \left[(\mathbf{B}_0 \cdot \nabla)^2 v_y \right] \hat{\mathbf{y}}. \quad (8)$$

Note that similar to Oliver et al. (1993), we consider MHD waves with $k_y = 0$ with k_y as the wavenumber in y -direction. Therefore, we also rule out the resonantly damped waves here.

B. The Governing Equation

Using $\mathbf{v}_1 = \frac{\partial \xi}{\partial t}$, we can write the y -component of the Equation (8) as:

$$\frac{d^2 \xi_y}{dx^2} + \left\{ \frac{\omega^2}{v_{A0}^2} \left[\cos \left(\frac{x_0}{H_B} \right) \right]^{\delta-2} \left[\cos \left(\frac{x}{H_B} \right) \right]^{-\delta} \right\} \xi_y = 0, \quad (9)$$

where, $\delta = \frac{H_B}{H_p}$ and $v_{A0} \left(= \frac{B_0}{\sqrt{\mu \rho_0}} \right)$ is the Alfvén speed at the base of the arcade. $(x_0, 0)$ is the coordinate of a particular field line. (see Tarr, 2017; Equation (30) in Oliver et al., 1993).

Note that the Alfvén speed $v_A(z)$ decreases with height for $0 \leq \delta < 2$ and $x/H_B < \pi/2$ otherwise $\cos(x/H_B)$ will make the coefficient infinite.

Let

$$\frac{x}{H_B} = \tilde{x}, \quad \frac{x_0}{H_B} = \tilde{x}_0. \quad (10)$$

Thus, Equation (9) can be written as:

$$\frac{d^2 \xi_y}{d\tilde{x}^2} + \left\{ k^2 \left[\cos(\tilde{x}_0) \right]^{\delta-2} \left[\cos(\tilde{x}) \right]^{-\delta} \right\} \xi_y = 0, \quad (11)$$

where

$$k = H_B \frac{\omega}{v_{A0}}. \quad (12)$$

1. No stratification due to gravity: $\delta \rightarrow 0$:

For $\delta \rightarrow 0$, H_p becomes very large and the gas pressure and density do not vary with height. Thus, for $\delta = 0$, Equation (11) reduces to

$$\frac{d^2 \xi_y}{d\tilde{x}^2} + k_x^2 \xi_y = 0; \quad k_x^2 = k^2 \cos^{-2}(\tilde{x}_0), \quad (13)$$

which has the following solutions:

$$\xi_y = A \cos(k_x^{(n)} \tilde{x}) \quad \text{with} \quad k_x^{(n)} = \frac{(n + \frac{1}{2})\pi}{\tilde{x}_0} \quad \text{for} \quad n = 0, 1, 2, \dots \quad (14)$$

and

$$\xi_y = A \sin(k_x^{(m)} \tilde{x}) \quad \text{with} \quad k_x^{(m)} = \frac{m\pi}{\tilde{x}_0} \quad \text{for} \quad m = 1, 2, \dots \quad (15)$$

such that $\xi_y = 0$ at $\tilde{x} = \pm \tilde{x}_0$.

This was the case considered by Tarr (2017).

2. Effect of stratification $\delta \neq 0$:

Through homogeneity, we use $\xi_y = 1$ at $\tilde{x} = 0$ in solving Equation (11) numerically. For a given δ and \tilde{x}_0 , we find k satisfying $\xi_y = 0$ at \tilde{x}_0 . In this model, the parameter \tilde{x}_0 indirectly measures the influence of density changes with height; smaller values of \tilde{x}_0 indicate low lying loops and hence less affected by density changes with height. The interesting cases are when the density is different at the base and at the loop-tops i.e. when the loop/arcade footpoints are far apart. As an example, we choose values of 0.5 (blue) 0.9 (black) for \tilde{x}_0 and solve the Equation (11). The resulting k values are shown in Figure 1 for the fundamental and the first four harmonics. The symbols plus, asterisk, diamond, triangle and cross are for 5 different values of δ of 0, 0.5 1.0, 2.0 and 3.0 respectively. Figure 1 clearly suggests that for these choice of parameter \tilde{x}_0 , the k values are lower for the higher value of \tilde{x}_0 and for each \tilde{x}_0 , the dimensionless k increases with δ compared with its value for the uniform density

This is the author's peer reviewed, accepted manuscript. However, the online version of record will be different from this version once it has been copyedited and typeset.

PLEASE CITE THIS ARTICLE AS DOI: 10.1063/1.50002512

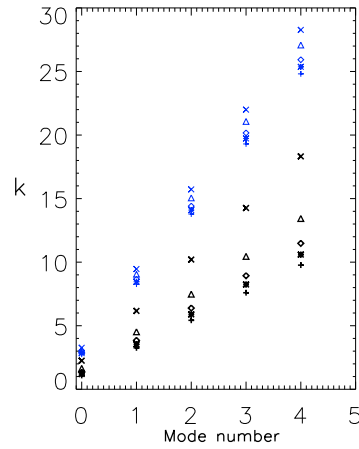


FIG. 1. Dimensionless eigenvalue k as a function of mode numbers for $\tilde{x}_0 = 0.5$ (blue/light) and 0.9 (black/dark): the x -axis denotes the fundamental mode (0), first (1), second (2), third (3) etc. harmonic modes. The symbols plus, asterisk, diamond, triangle and cross are for the δ values of 0, 0.5, 1.0, 2.0 and 3.0 respectively.

case (recall that uniform density case is when $\delta = 0$). Also, note that the shift is larger for higher harmonic index or mode number.

In Figure 2 we show the first four harmonics of the normalised eigenfunctions for $\tilde{x}_0 = 1.3$, for three different values of δ . We have discrete oscillations on a given field line but the nodes will be shifted for different field lines (i.e. for different x_0) as suggested from Figure 1. Thus, if seen from above an arcade consisting of many field lines of different lengths and separations could yield a continuous frequency spectrum for excited Alfvén waves.

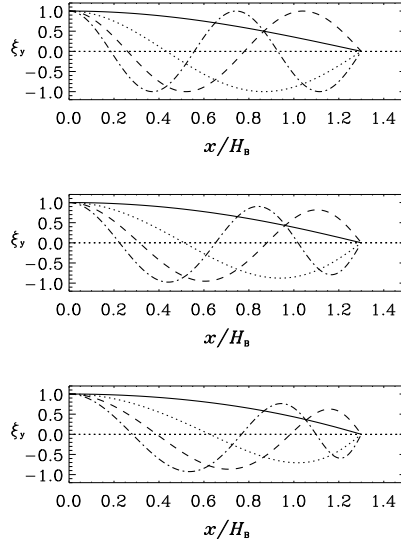


FIG. 2. Normalised eigenfunction as a function of x/H_B for $\delta = 0$ (top), 1, and 2 (bottom). Here $\tilde{x}_0 = 1.3$ is used. The solid, dotted, dashed and dot-dashed lines are for fundamental, first, second and third harmonics respectively.

III. EXCITATION OF ALFVÉN MODES BY AN INITIAL PERTURBATION

Tarr (2017) investigated the excitation of the Alfvén modes by an initial Gaussian perturbation at the loop-top. Here, we consider an even function of the form

$$\xi_y(\tilde{x}) = \frac{\cos\left(\frac{\pi\tilde{x}}{2\tilde{x}_0}\right)}{\sqrt{2\pi}\sigma} e^{-\frac{\tilde{x}^2}{2\sigma^2}}, \quad (16)$$

for a small finite width σ . This function vanishes at the line-tied boundaries. Such a perturbation is quite restricted and can be envisaged at the top of the loop when the magnetic reconnection occurs there and perturbs the loop tops. When projected onto the even perturbations $\xi_y(= Y)$ obtained from solving the Equation (11), yields

$$\xi_y(\tilde{x}) = \sum_{i=0}^{\infty} A_i Y_i(\tilde{x}). \quad (17)$$

This is the author's peer reviewed, accepted manuscript. However, the online version of record will be different from this version once it has been copyedited and typeset.

PLEASE CITE THIS ARTICLE AS DOI: 10.1063/5.0002512

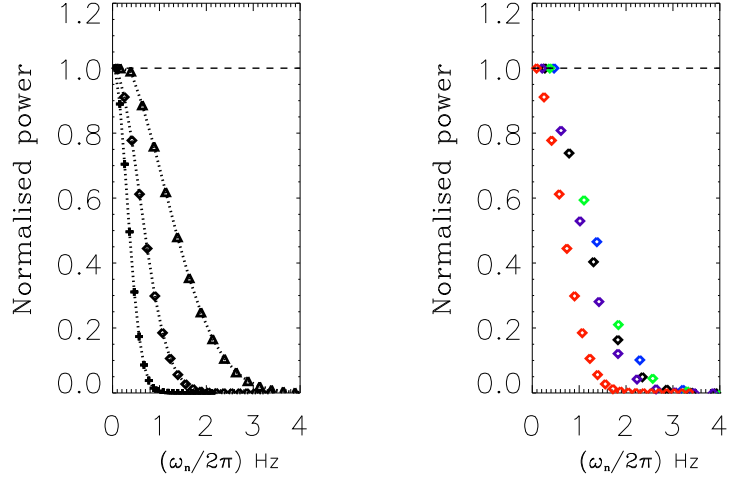


FIG. 3. Normalised power as a function of $\omega_n/2\pi$. *Left:* for $\tilde{x}_0=1.3$ showing $\delta = 0$ (plus), 1 (diamond) and 2 (triangle). *Right:* $\delta = 1$ for $\tilde{x}_0=1.3$ (red), 0.9 (purple), 0.77 (black), 0.6 (green) and 0.5 (blue). Here, all values are computed for $\sigma = 0.1$.

The amplitude A_n can be given by

$$A_n = \int_{-\tilde{x}_0}^{\tilde{x}_0} w(\tilde{x})\xi_y(\tilde{x})Y_n(\tilde{x})d\tilde{x}, \quad (18)$$

where $w(x) = [\cos(\tilde{x})]^{-\delta}$ is the weighting function. For the purpose of finding the amplitude, we have taken the normalisation as

$$\int_{-\tilde{x}_0}^{\tilde{x}_0} w(\tilde{x})[Y_n(\tilde{x})]^2d\tilde{x} = 1. \quad (19)$$

The frequency power spectrum can be plotted as A_n^2 , as a function of $\frac{\omega_n}{2\pi}$, where ω_n is obtained from different eigenvalues.

We plot the normalised power as a function of this frequency $\omega_n/2\pi$ in Figure 3. In the left panel, we examine the effect of parameter δ on the frequency power spectrum for one field line so we fix $\tilde{x}_0 = 1.3$ and plot the normalised power for $\delta = 0$ (plus), 1 (diamond) and 2 (triangle). It is clear from the Figure that for all three values of δ , the power decreases

with increasing harmonic index with substantial power up to 1.5 Hz for higher δ . When $\delta = 0$, the effect of gravity is zero resulting in a constant gas pressure everywhere and plasma β increasing with height. In fact, the plasma $\beta = 2\mu\frac{p}{B_0^2}e^{\frac{\tilde{x}}{H_B}(2-\delta)}$ increases with height for $0 \leq \delta < 2$ with the rate slowing down with higher values of δ within this range. When $\delta = 2$, the magnetic pressure and the gas pressure decay with height at the same rate and thus, the basic equilibrium has a constant plasma β . We therefore, examined and compared frequency spectrum for three values of $\delta = 0, 1$ and 2 to study the effect of varying plasma beta.

Recall that the perturbation is a Cosine-modulated Gaussian function (i.e. $\xi_y(\tilde{x}) = \frac{\cos(\frac{\tilde{x}\tilde{x}}{2\tilde{x}_0})}{\sqrt{2\pi}\sigma}e^{-\frac{\tilde{x}^2}{2\sigma^2}}$). We first examine the frequency power spectrum for many field lines in an arcade resulting from this perturbation. This would give us an idea about the frequency-power spectrum for a collection of field lines with different separations in an arcade when viewed from above. Oliver et al. (1993) suggest that $\delta \approx 1$ is appropriate for coronal conditions. So, in the right panel of Figure 3, we show normalised power for a fixed $\delta (= 1)$ and choose parameters $\tilde{x}_0 = 1.3$ (red), 0.9 (purple), 0.77 (black), 0.6 (green) and 0.5 (blue). The peak amplitude occurs at a fundamental frequency which is relatively low (< 1 Hz). For higher harmonics, the power appears to increase slightly with \tilde{x}_0 due to the shift in frequency (refer to Figure 1). The effect of varying \tilde{x}_0 is that it shifts the eigenvalues and hence the presence of many different \tilde{x}_0 in an arcade will yield a continuous spectrum if the arcade is seen from above as one entity.

It would be interesting to compare the power spectrum for an arcade in an atmosphere where the plasma β decreases with height. This requires choosing $\delta > 2$. We expect the effect to be more apparent for higher loops (i.e. larger values of \tilde{x}_0) in the arcade. In Figure 4, we plot normalised power as a function of $\omega_n/2\pi$ for $\delta = 2.5$ (plus), 2.7 (diamond) and 3 (asterisk) in the left panel. Here, $\tilde{x}_0 = 1.3$ is kept fixed. The power is normalised by the maximum value which occurs for the first harmonic instead of for the fundamental mode. In the right panel, we show the normalised power for a fixed value of $\delta = 3$ for different \tilde{x}_0 . It is clear from the figure that for the wider loops (refer to $\tilde{x}_0 = 1.2$ and 1.3), we see higher power for all harmonics with substantial power even at high frequencies ($\nu > 3$). Once again, it can be inferred that an arcade will yield a continuous spectrum if the arcade is seen from above as one entity with fluctuations in this continuous spectrum depending on various sizes of the loop comprising the arcade.

This is the author's peer reviewed, accepted manuscript. However, the online version of record will be different from this version once it has been copyedited and typeset.

PLEASE CITE THIS ARTICLE AS DOI: 10.1063/5.0002512

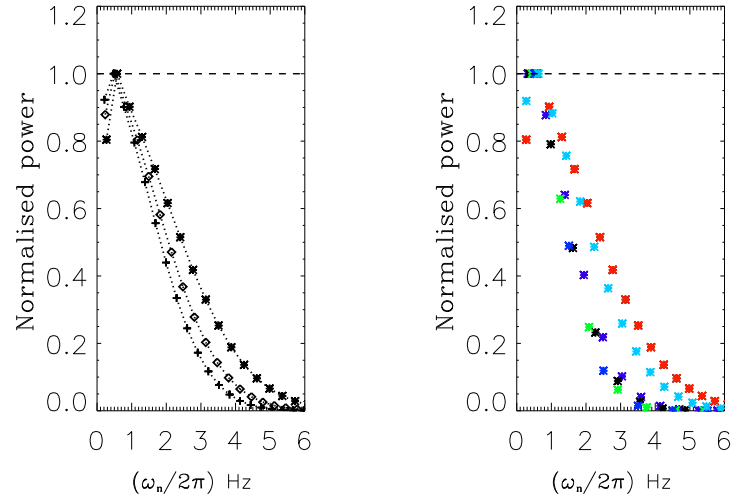


FIG. 4. Normalised power as a function of $\omega_n/2\pi$. *Left*: for $\tilde{x}_0=1.3$ showing $\delta = 2.5$ (plus), 2.7 (diamond) and 3.0 (asterisk). *Right*: $\delta = 3$ for $\tilde{x}_0=1.3$ (red), 1.2 (turquoise), 0.9 (purple), 0.77 (black), 0.6 (green) and 0.5 (blue). Here, all values are computed for $\sigma = 0.1$.

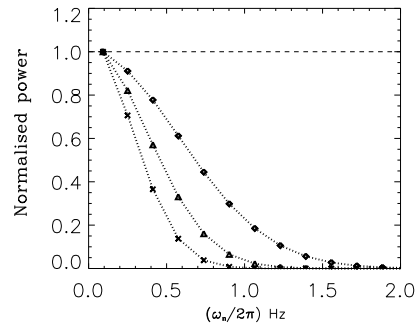


FIG. 5. Normalised power as a function of $\omega_n/2\pi$: for $\tilde{x}_0=1.3$ and $\delta = 1$. The values of σ are 0.1 (diamond), 1.5 (triangle) and 0.2 (cross).

This is the author's peer reviewed, accepted manuscript. However, the online version of record will be different from this version once it has been copyedited and typeset.

PLEASE CITE THIS ARTICLE AS DOI: 10.1063/1.50002512

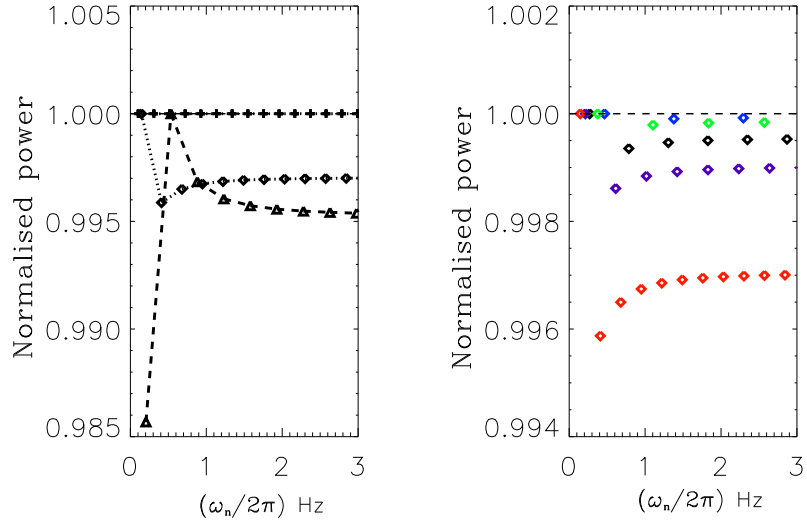


FIG. 6. Normalised power as a function of $\omega_n/2\pi$ for an impulsive driver. *Left*: for $\tilde{x}_0=1.1$ showing $\delta = 0$ (plus), 1 (diamond) and 2 (triangle). *Right*: $\delta = 1.0$ for $\tilde{x}_0=1.1$ (red), 0.9 (purple), 0.77 (black), 0.6 (green) and 0.5 (blue). Here, all values are computed for $\sigma = 0.1$.

Now, we examine the size of the perturbation that drives the oscillations. In Figure 5, we investigate the effect of the size of the perturbation on the power spectrum. To do this, we fix the size of the field line with $\tilde{x}_0 = 1.3$ and also fix the scale-heights in the background atmosphere with $\delta = 1$. We show the computed normalised power spectrum for three values of $\sigma = 0.1$ (diamond), 0.15 (triangle) and 0.2 (cross). It is clear that the power is more focussed in the lower frequency range for higher value of σ . This suggests that from the observed power spectra of the same-width loops, the size of the perturbation can be constrained.

The oscillations in the solar corona are often observed in response to a nearby big flare (Aschwanden et al. 1999; Nakariakov et al. 1999). Thus, another driver that is worth investigating in the context of the flare-induced oscillations is an impulsive driver. In Figure 6, we plot the normalised power for a perturbation function as the Dirac-delta function. Note that the power is almost constant with frequency except for some fluctuations at very

low frequencies for stratified atmosphere (i.e. $\delta > 0$) or for longer loops (i.e. larger \tilde{x}_0).

IV. CONCLUSION

In this paper, we have computed the frequency spectrum of Alfvén waves excited by a Cosine-modulated Gaussian perturbation at the top of a set of solar coronal loops (see Tarr (2017)). The loops were modelled as two-dimensional potential magnetic field embedded in a stratified plasma atmosphere in the ideal MHD framework. The governing equation, derived from the linearised momentum equation, was solved numerically for the line-tied boundary conditions. The important stratification parameter, δ which measures the relative strength of the magnetic and gas pressure scale heights was varied to study the eigenvalues and the corresponding eigenfunctions.

An initial perturbation, a Cosine-modulated Gaussian wavefunction, was then projected onto the even eigenfunctions to compute the power spectrum. The power spectrum suggests that Alfvén waves excited by a Gaussian perturbation at the coronal loop-top contain substantial power up to several Hz depending on the choice of parameters such as the arcade width, length, Alfvén speed at the photosphere $z = 0$ and the distribution of plasma β in the equilibrium atmosphere (through the value of δ).

The power spectra are completely different for an impulsive driver, with the low frequency distribution affected more with the parameter δ . The normalised power are almost constant for higher harmonic index but for an arcade seen from above as a single entity, the nature of the power spectrum for the first two-three harmonics will be dominated by the widths of the field lines in this entity. To distinguish the type of driver that excite Alfvén modes in a solar coronal arcade, it would require observing many higher harmonics. Such high frequency Alfvén spectra resulting from different drivers can only be observed in realistic coronal conditions if the observational data can be obtained with a very high temporal cadence and frequency resolution. For example, a temporal cadence of 3-4 second would be useful which is around one third of what is currently available from Atmospheric Imaging Assembly (AIA) on board the Solar Dynamics Observatory (SDO) (see Lemen et al. 2012). The nature of the power spectra can, in principle, constrain the size and type of the driver.

We demonstrated that the oscillating modes are discrete for a given field line and depending on the eigenvalues for each field line in an arcade, a continuous spectrum of frequency

This is the author's peer reviewed, accepted manuscript. However, the online version of record will be different from this version once it has been copyedited and typeset.

PLEASE CITE THIS ARTICLE AS DOI: 10.1063/1.50002512

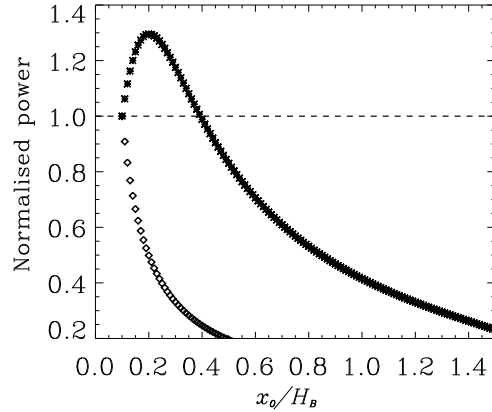


FIG. 7. Normalised power as a function of $\tilde{x}_0 \left(= \frac{x_0}{H_B} \right)$ for the fundamental mode. The asterisks and diamonds are for the Gaussian and impulsive driver respectively. The value of σ is chosen to be 0.1 and both the curves are for the $\delta = 1$ case.

for Alfvén waves may be expected if observed from above (see also, Oliver et al. (1993)). Thus, the discrete and continuous nature of frequency spectrum depends on the orientation of the field lines in an arcade and the line-of-sight of the observations. The quantitative behaviour also depends on the type of the driver. As an illustration, we plot in Figure 7 normalised power as a function of $\tilde{x}_0 \left(= \frac{x_0}{H_B} \right)$ for the fundamental mode. The value of σ chosen is 0.1. Both curves are for $\delta = 1$ case. It is clear from the Figure that the frequency power spectrum appears continuous for both drivers but with different magnitudes for the same bundle of field lines.

It is worth noting that in this study, we neglected plasma pressure perturbation and hence there are no slow waves. Kaneko et al. (2015) studied the interesting phenomenon of superslow propagation of Alfvén and slow continuum waves. Using the model of Oliver et al. (1993) they reported that Alfvén and slow wave continua can get phase-mixed with time and the process gives an impression of fast wave propagation across the magnetic surface despite the speed of propagation slower than the local Alfvén/sound speed. They also derived the phase velocity which revealed that the phase speed decreases with height and the strong change occurs for low height (i.e. for low-lying loops). One of the key findings of Kaneko

This is the author's peer reviewed, accepted manuscript. However, the online version of record will be different from this version once it has been copyedited and typeset.

PLEASE CITE THIS ARTICLE AS DOI: 10.1063/1.50002512

et al. (2015) is that the apparent propagation is inversely proportional to time, thereby suggesting that waves are fast soon after the excitation and a slow(fast) spatial change in the local Alfvén frequency causes a rapid (slow) propagation. In our future study, we will consider the effects of plasma pressure.

Availability of Data

The data that support the findings of this study are available from the corresponding author upon request.

REFERENCES

- Aschwanden, M. J., Fletcher, L., Schrijver, C. J., & Alexander, D. 1999, *The Astrophysical Journal*, 520, 880
- De Groof, A. and Goossens, M. 2002, *A&A*, 386, 691-69
- Diaz, A. J., Oliver, R., Ballester, J. L., & Roberts, B. 2004, *A&A*, 424, 1055
- Edwin, P. M. & Roberts, B. 1982, *Solar Physics*, 76, 239-259
- Edwin, P. M. & Roberts, B. 1983, *Solar Physics*, 88, 179-191
- Goossens, M., Andries, J., & Aschwanden, M. J. 2002, *A&A*, 394, 39
- Heyvaerts, J., Priest, E. R. 1983, *A&A*, Vol. 117, 220-234
- Hindman, B. W. & Jain, R. 2015, *The Astrophysical Journal*, 784, 103
- Hindman, B. W. & Jain, R. 2018, *The Astrophysical Journal*, 858, 6
- Jain, R., Maurya, A. R., and Hindman, B. W. 2015, *The Astrophysical Journal Letters*, 804, L19
- Kaneko, T. , Goossens, M., Soler, R., Terradas, J., van Doorselaere, T. Yokoyama, T. and Wright A. 2015, *The Astrophysical Journal*, 812, 121
- Lemen, J. R., Title, A. M., Akin, D. J., Boerner, P. F., Chou, C., Drake, J. F., Duncan, D. W., Edwards, C. G., Friedlaender, F. M., Heyman, G. F. et al. 2012, *Solar Physics*, 275, 17
- Li, H., Liu, Y., and Tam, K. V. 2017, *The Astrophysical Journal*, 842, 99
- Nakariakov, V. M., Ofman, L., Deluca, E. E., Roberts, B., & Davila, J. M. 1999, *Science*, 285, 862
- Oliver, R., Ballester, J. L., Hood, A. W. & Priest, E. R. 1993, *A&A*, 273, 647
- Pesnell, W. D., Thompson, B. J., & Chamberlin, P. C. 2012, *Solar Physics*, 275, 3
- Roberts, B. 1981, *Solar Physics*, 69, 39

This is the author's peer reviewed, accepted manuscript. However, the online version of record will be different from this version once it has been copyedited and typeset.

PLEASE CITE THIS ARTICLE AS DOI: 10.1063/5.0002512

Soler, R., Oliver, R. & Ballester, J. L. 2008, *The Astrophysical Journal*, 684, 725

Tarr, L. A. 2017, *The Astrophysical Journal*, 847, 1

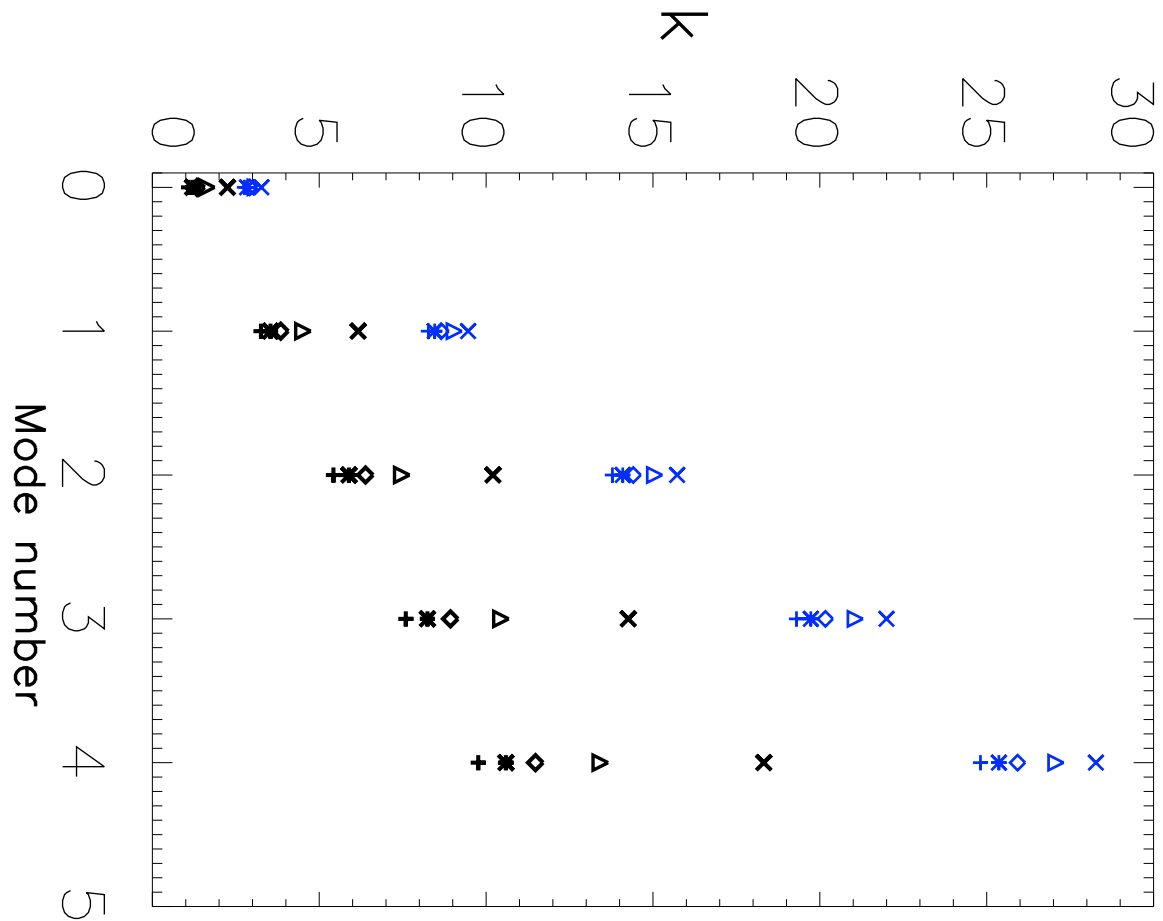
Terradas, I. A. J., Oliver, R. & Ballester, J. L. 2007, *A&A*, 466, 1145-1151

Verwichte, E., Nakariakov, V. M., Ofman L. & DeLuca, E. E. 2004, *Solar Physics*, 223, 77

White, R. S. & Verwichte, E. 2012, *A&A*, 537, A49

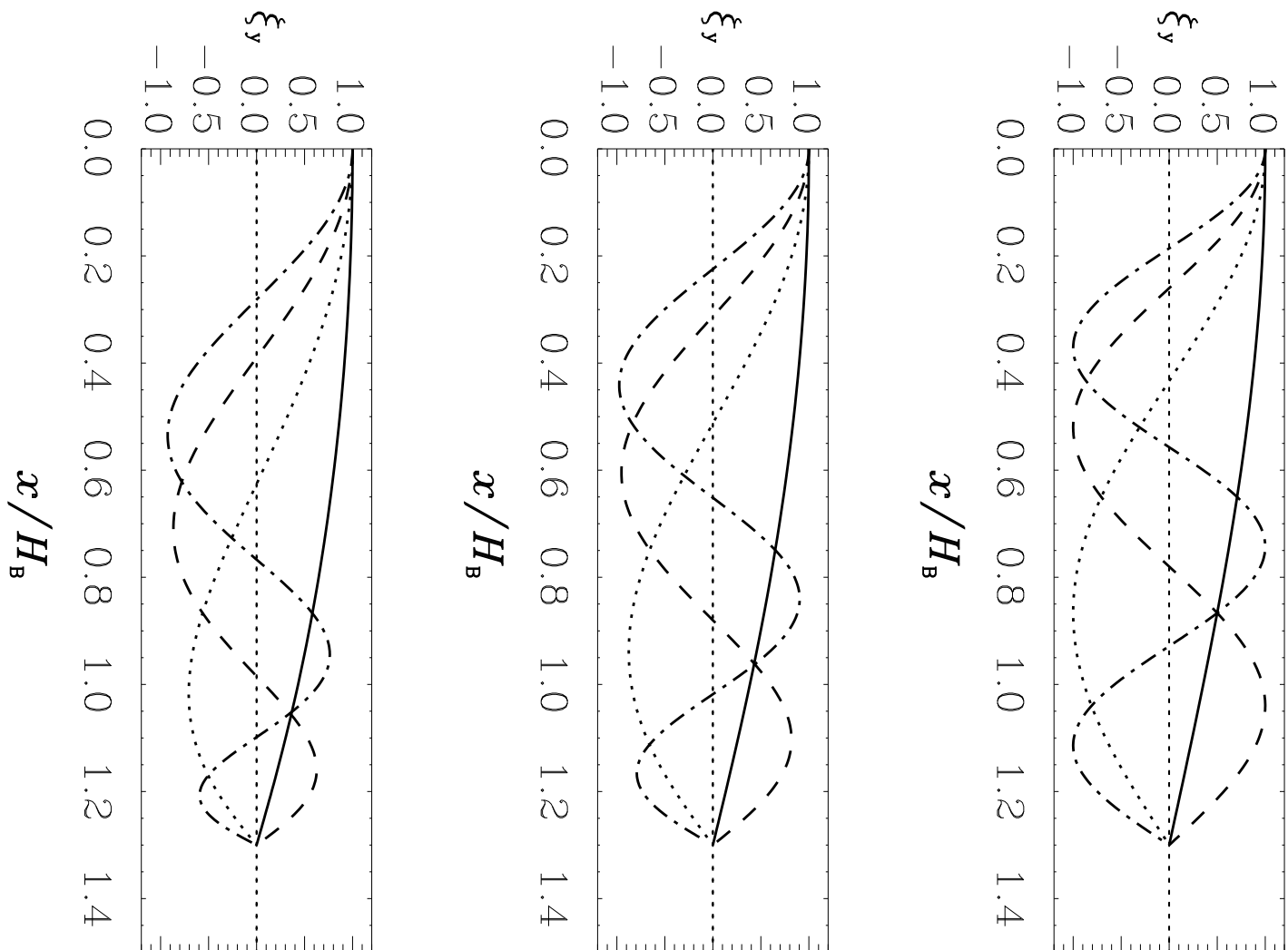
This is the author's peer reviewed, accepted manuscript. However, the online version of record will be different from this version once it has been copyedited and typeset.

PLEASE CITE THIS ARTICLE AS DOI: 10.1063/5.0002512



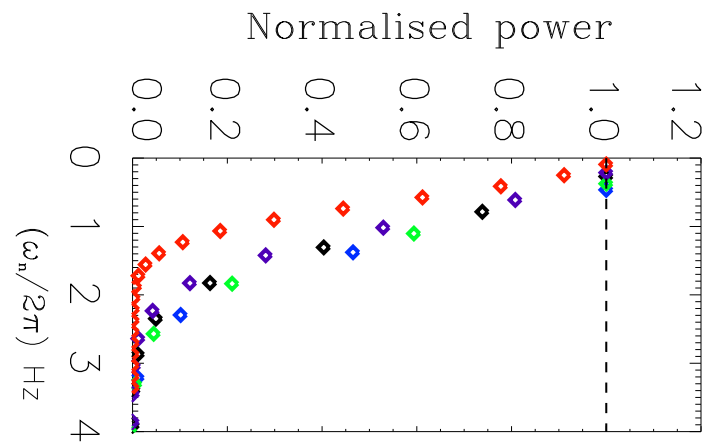
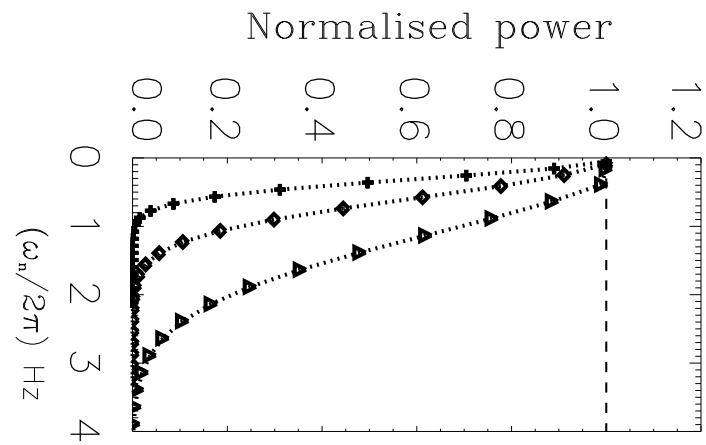
This is the author's peer reviewed, accepted manuscript. However, the online version of record will be different from this version once it has been copyedited and typeset.

PLEASE CITE THIS ARTICLE AS DOI: 10.1063/5.0002512



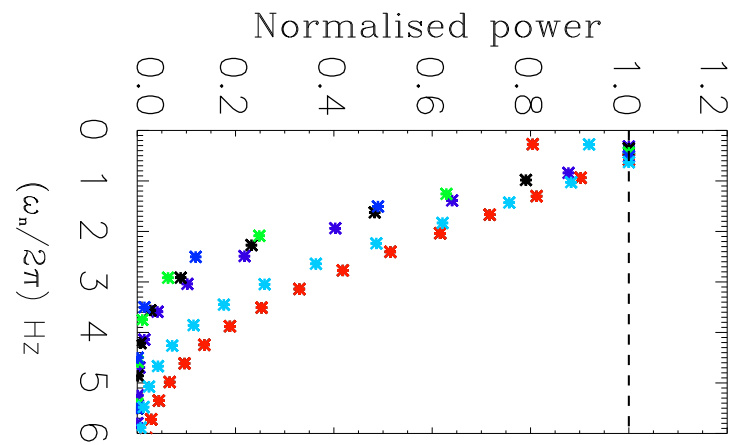
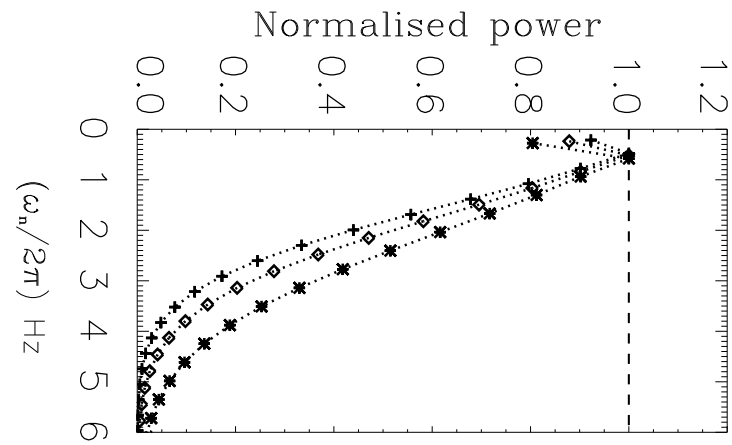
This is the author's peer reviewed, accepted manuscript. However, the online version of record will be different from this version once it has been copyedited and typeset.

PLEASE CITE THIS ARTICLE AS DOI: 10.1063/5.0002512



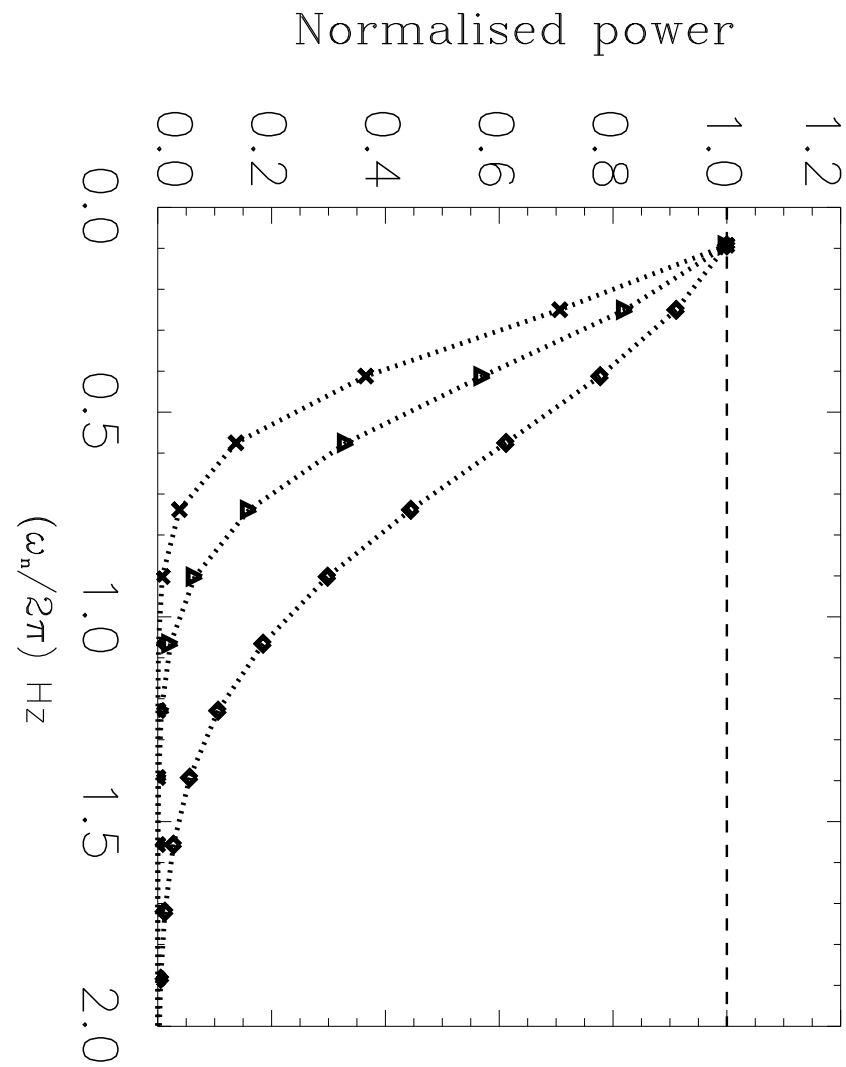
This is the author's peer reviewed, accepted manuscript. However, the online version of record will be different from this version once it has been copyedited and typeset.

PLEASE CITE THIS ARTICLE AS DOI: 10.1063/5.0002512



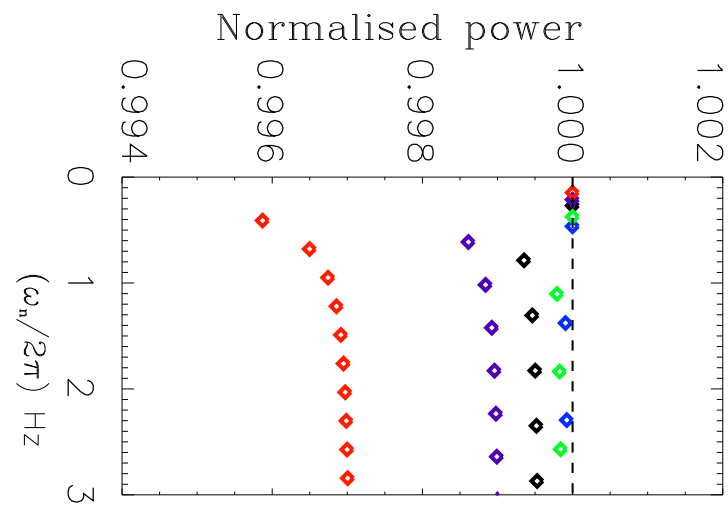
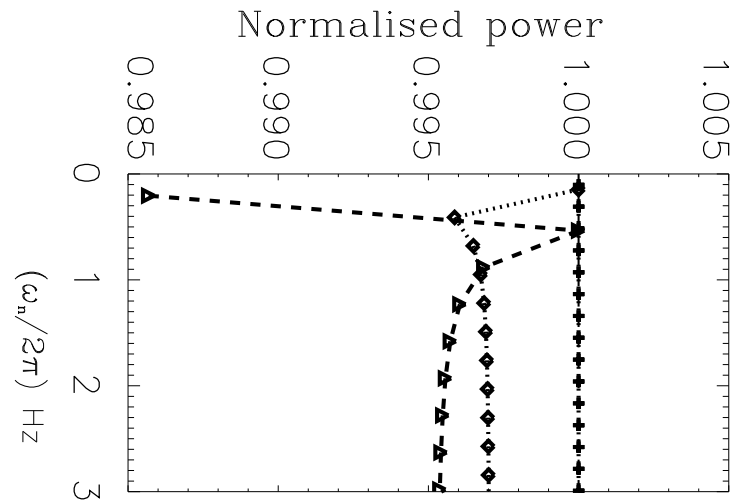
This is the author's peer reviewed, accepted manuscript. However, the online version of record will be different from this version once it has been copyedited and typeset.

PLEASE CITE THIS ARTICLE AS DOI: 10.1063/5.0002512



This is the author's peer reviewed, accepted manuscript. However, the online version of record will be different from this version once it has been copyedited and typeset.

PLEASE CITE THIS ARTICLE AS DOI: 10.1063/5.0002512



This is the author's peer reviewed, accepted manuscript. However, the online version of record will be different from this version once it has been copyedited and typeset.

PLEASE CITE THIS ARTICLE AS DOI: 10.1063/5.0002512

